nature biotechnology

Intravascular AAV9 preferentially targets neonatal neurons and adult astrocytes

Kevin D Foust[1], Emily Nurre[1,2], Chrystal L Montgomery[1], Anna Hernandez[3], Curtis M Chan[3] & Brian K Kaspar[1,2]

Delivery of genes to the brain and spinal cord across the blood-brain barrier (BBB) has not yet been achieved. Here we show that adeno-associated virus (AAV) 9 injected intravenously bypasses the BBB and efficiently targets cells of the central nervous system (CNS). Injection of AAV9-GFP into neonatal mice through the facial vein results in extensive transduction of dorsal root ganglia and motor neurons throughout the spinal cord and widespread transduction of neurons throughout the brain, including the neocortex, hippocampus and cerebellum. In adult mice, tail vein injection of AAV9-GFP leads to robust transduction of astrocytes throughout the entire CNS, with limited neuronal transduction. This approach may enable the development of gene therapies for a range of neurodegenerative diseases, such as spinal muscular atrophy, through targeting of motor neurons, and amyotrophic lateral sclerosis, through targeting of astrocytes. It may also be useful for rapid postnatal genetic manipulations in basic neuroscience studies.

Nearly all large-molecule drugs and ~98% of small-molecule drugs do not cross the BBB, limiting the development of drugs for many disorders of the CNS[1]. Gene therapy has been proposed as a means of crossing the BBB[2]; however, widespread delivery to the brain and spinal cord has proved challenging. Successful gene therapies for motor neuron disease are expected to require broad transduction within the spinal cord and motor cortex. Two of the most common motor neuron diseases are spinal muscular atrophy (SMA) and amyotrophic lateral sclerosis (ALS), debilitating disorders of children and adults, respectively, with no effective therapies to date. Recent work in rodent models of SMA and ALS have demonstrated the potential of gene delivery using viruses that undergo retrograde transport after intramuscular injection, and this approach is currently being explored for clinical trials[2–5]. However, clinical development may be difficult given the numerous injections that would be required to target the widespread regions of neurodegeneration throughout the spinal cord, brainstem and motor cortex observed in these diseases. AAV vectors such as AAV2 have shown promise in several recent clinical trials for neurological disorders, demonstrating sustained transgene expression, a relatively safe profile and promising functional responses, yet have required surgical intraparenchymal injections[6–8].

Newly discovered AAV serotypes, particularly AAV6, AAV8 and AAV9, have led to advances in delivery, allowing widespread transduction throughout multiple tissues, such as skeletal and cardiac muscle, after simple systemic intravenous or intraperitoneal injections[9–13]. These serotypes have all been shown to cross vascular endothelial cell barriers efficiently. However, vascular delivery approaches to target lower motor neurons (LMNs) or other cell types within the CNS have been inefficient, probably because the viral vectors cannot cross the BBB. AAV serotypes 6 and 8 showed poor penetration of the CNS after vascular gene delivery in neonatal and adult mice, being expressed in only a few cells within the spinal cord[14,15]. AAV9, however, appears to possess unique serological characteristics. Neutralizing antibodies created against AAV serotypes 1–8 showed little to no cross-reactivity with AAV9, indicating that AAV9 is of a different AAV clade[16]. Furthermore, after intraparenchymal injection, AAV9 is more readily transported within the brain compared with other AAV serotypes[17]. AAV9 is known to use the laminin receptor, as do AAV2 and AAV8 but not AAV6, and may use other unknown receptors for cell attachment, internalization and transduction[18]. Therefore, AAV9 may have varied capsid topography and target-cell interactions.

Given the unique properties of AAV9 (refs. 16–18), we investigated whether this serotype could efficiently deliver genes to the CNS after intravenous injection in neonatal mice, where the BBB is not fully developed, and in adult mice, where the BBB is fully formed. We injected neonates in the facial vein and adults in the tail vein using AAV9 vectors that express green fluorescent protein (GFP). In neonates, a single intravascular AAV9 injection led to extensive transduction in dorsal root ganglia and motor neurons in spinal cord and in neurons in most brain regions. In adults, transduction occurred predominantly in astrocytes in both spinal cord and brain.

RESULTS

Intravenous injection in neonates targets motor neurons

To evaluate transduction of LMNs, we first investigated transgene expression after intravenous injection in neonatal mice, before the closure of the BBB. One-day-old wild-type mice received temporal vein injections of 4×10^{11} particles of a self-complementary AAV9

[1]Center for Gene Therapy, The Research Institute at Nationwide Children's Hospital, 700 Children's Drive, Columbus, Ohio 43205, USA. [2]Department of Pediatrics, College of Medicine, The Ohio State University, 700 Children's Drive, Columbus, Ohio 43205, USA. [3]Special Pathology Services, Charles River, Preclinical Services Nevada, 6995 Longley Lane, Reno, Nevada 89511, USA. Correspondence should be addressed to B.K.K. (brian.kaspar@nationwidechildrens.org).

Received 30 September; accepted 24 November; published online 21 December 2008; doi:10.1038/nbt.1515

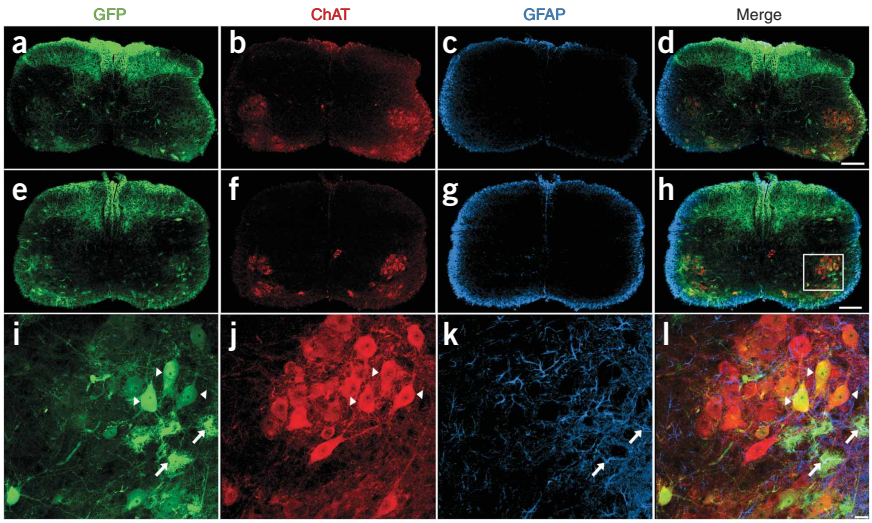

Figure 1 Intravenous injection of AAV9 leads to widespread neonatal spinal cord transduction. (**a**–**l**) Cervical (**a**–**d**) and lumbar (**e**–**l**) spinal cord sections 10 d after facial-vein injection of 4×10^{11} particles of scAAV9-CB-GFP into postnatal-day-1 mice ($n = 8$). GFP expression (**a**,**e**,**i**) was predominantly restricted to LMNs (**a**,**e**,**i**) and fibers that originated from DRG (**a**,**e**). GFP-positive astrocytes (**i**,**l**, arrows) were also observed scattered throughout the tissue sections. LMN and astrocyte expression were confirmed by co-localization using ChAT (**b**,**f**,**j**) and GFAP (**c**,**g**,**k**), respectively. Merged images of GFP, ChAT and GFAP (**d**,**h**,**l**). A z-stack image (**i**–**l**) of the area within the box in **h** shows the extent of LMN (arrow heads) and astrocyte (arrows) transduction within the lumbar spinal cord. Scale bars, 200 μm (**d**,**h**), 20 μm (**l**).

(scAAV9) vector[19] that expresses green fluorescent protein (GFP) under the control of the chicken β-actin hybrid promoter (CB). Animals were euthanized 10 or 21 d post-injection, and brains and spinal cords were evaluated for transgene expression. Robust GFP expression was found in heart and skeletal muscles as expected (data not shown). Spinal cords showed GFP expression throughout, with robust GFP expression in fibers that ascended in the dorsal columns and fibers that innervated the spinal gray matter, indicating dorsal root ganglia (DRG) transduction. GFP-positive cells were also found in the ventral region of the spinal cord where LMNs reside (**Fig. 1**). Co-labeling for choline acetyl transferase (ChAT) and GFP expression within the spinal cord revealed a large number of ChAT-positive cells expressing GFP throughout all cervical and lumbar sections examined, indicating widespread LMN transduction (**Fig. 1l** and **Supplementary Fig. 1** online). Approximately 56% of ChAT-positive cells strongly expressed GFP in sections of the lumbar spinal cord of 10-d-old mice and ~61% of 21-d-old mice, demonstrating early and persistent transgene expression in LMNs (**Table 1**). Similar numbers of LMN expression were seen in cervical and thoracic regions of the spinal cord. To our knowledge, this is the highest proportion of LMNs

Table 1 Counts of neurons transduced in neonates and phenotypic evaluation of cells transduced in adult mice

		Neonate		
		GFP (mean ± s.e.m.)	NeuN (mean ± s.e.m.)	% (mean ± s.e.m.)
Brain	Retrosplenial/cingulate			
	10 d post-injection	108,232 ± 6,677	684,909 ± 15,293	15 ± 0.9
	21 d post-injection	142,658 ± 11,124	762,104 ± 38,397	18 ± 1.9
	Dentate gyrus			
	10 d post-injection	26,978 ± 2,568	228,184 ± 21,835	11 ± 0.5
	21 d post-injection	42,304 ± 15,613	278,043 ± 11,383	14 ± 4.8
	Purkinje cells			
	10 d post-injection	46,505 ± 8,885	71,740 ± 6,049	64 ± 8.2
	21 d post-injection	52,720 ± 1,951	73,814 ± 5,220	71 ± 3.0
Lumbar spinal cord		GFP (mean ± s.e.m.)	ChAT (mean ± s.e.m.)	% (mean ± s.e.m.)
	10 d post-injection	149 ± 31	264 ± 53	56 ± 1.9
	21 d post-injection	83 ± 16	140 ± 31	60 ± 2.9
		Adult		
		GFP (mean ± s.e.m.)	GFAP (mean ± s.e.m.)	% (mean ± s.e.m.)
Lumbar spinal cord (gray matter)	GFP co-labeled w/GFAP	48 ± 10	43 ± 7	91 ± 4.8
	GFAP-positive transduced	41 ± 5	64 ± 8	64 ± 0.9

For neonatal injected mice, unbiased stereological evaluation of AAV9-transduced neurons were performed for three brain regions; retrosplenial/cingulate, dentate gyrus, and Purkinje cells and for the lumbar spinal cord at 10 d and 21 d post-injection. For adult mice, the percent of GFP-positive cells, co-labeled with astrocytic marker; GFAP, was analyzed. Extent of astrocytic transduction was also measured as the percent of GFAP-positive astrocytes expressing GFP. Means ± s.e.m. were reported with rounding to nearest whole number. Percentages ± s.e.m. were calculated. Student's *t*-tests were performed between 10- and 21-d time points for all regions analyzed demonstrating no significant differences between time points ($n = 4$–5 mice per time point, $P \geq 0.05$).

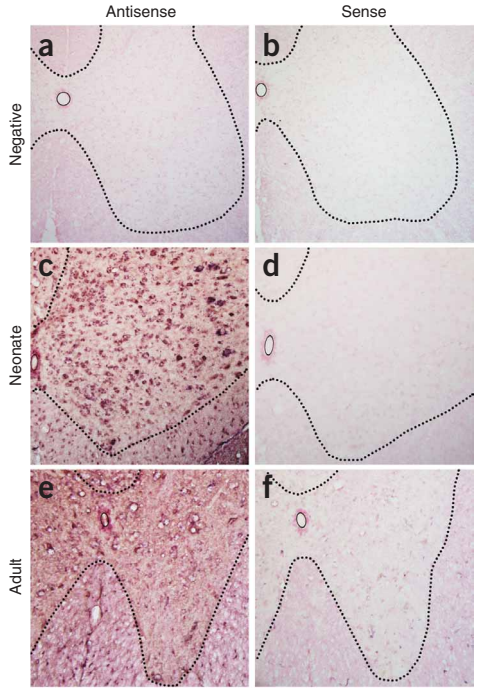

Figure 2 *In situ* hybridization of spinal cord sections from neonatal and adult mice injected with scAAV9-CB-GFP demonstrates that cells expressing GFP have been transduced. (**a**–**b**) Negative control mice injected with PBS showed no positive signal ($n = 2$). (**c**–**f**) Antisense probes for GFP, however, demonstrated strong positive signals for neonate ($n = 3$) (**c**) and adult ($n = 3$) (**e**) sections. No positive signals were found for the sense control probe in neonate (**d**) or adult (**f**) spinal cord sections. Tissues were counterstained with Nuclear Fast Red for contrast; probe hybridization is in purple.

transduced by a single injection of AAV reported. In addition to widespread DRG and LMN transduction, we observed GFP-positive glial cells throughout the spinal gray matter, indicating that an AAV9-delivered transgene with the CB promoter can be expressed in astrocytes (**Fig. 1l**). In addition to some astrocyte transduction, we also observed occasional transduced microglial cells in injected neonatal mice (**Supplementary Fig. 2** online). *In situ* hybridization performed with riboprobes against the viral construct on frozen spinal cord tissue confirmed that viral transcription, and not protein uptake, was responsible for the previously unseen transduction pattern (**Fig. 2**).

Injection in neonates targets neurons and astrocytes in brain

We next examined the brain after intravenous injection of scAAV9-CB-GFP on postnatal day 1 and found extensive GFP expression in all regions analyzed, including the striatum, cortex, anterior commissure, internal capsule, corpus callosum, hippocampus and dentate gyrus, midbrain and cerebellum (**Fig. 3a–h**, respectively, **Fig. 4a–d**). GFP-positive cells included neurons and astrocytes throughout the brain. We further characterized the transduced neurons by analyzing brain colabeling with GFP and GAD67, a GABAergic marker. The cortex, hippocampus and dentate had very little co-localization of GFP- and GAD67-labeled cells (**Supplementary Fig. 3a–i** online), whereas Purkinje cells in the cerebellum were extensively co-labeled (**Supplementary Fig. 3j–l** online). Finally, unbiased estimated stereological quantification of transduction showed that 15% ± 0.9% within the retrosplenial/cingulate cortex, 11% ± 0.5% within the dentate gyrus and 64% ± 8.2% within the Purkinje layer of total neurons were transduced 10 d post-injection. The percent of transduced neurons increased to 18% ± 1.9% within the retrosplenial/cingulate cortex, 14% ± 4.8% within the dentate gyrus and 71% ± 3.0% within the Purkinje layer 21 d after a one-time administration of virus (**Table 1**). The increase at 21 d post-injection was probably due to an increase in the gene expression detected because of accumulated GFP protein. However, the differences detected 10 or 21 d post-injection were not statistically different ($P > 0.05$), demonstrating stable transgene expression over time.

Mode of viral entry into the CNS

The pattern of GFP expression observed after intravenous administration on postnatal day 1 suggests two independent modes of viral entry into the CNS. Ubiquitous GFP expression throughout the brain indicates that the virus probably crosses the developing BBB. However, the GFP-expression pattern in the neonatal spinal cord is defined with respect to specific DRG and LMN transduction. The DRG and LMNs have projections into the periphery, suggesting that retrograde transport may be the mechanism of transduction. In support of this hypothesis, there were no GFP-positive interneurons observed in any section examined (**Fig. 1d,h**). Alternatively, the virus may have an LMN tropism after crossing the BBB, but this appears unlikely as ChAT-positive cells still migrating from the central canal to the ventral horn were largely untransduced (**Fig. 1d,h**). We tested whether AAV9 has the property of enhanced retrograde transport in adult mice by direct intramuscular injection of the vector into adult gastrocnemius muscles. Gene expression was high in myofibers but negligible in LMNs, suggesting that AAV9 does not undergo enhanced retrograde transport in adult mice (**Supplementary Fig. 4** online).

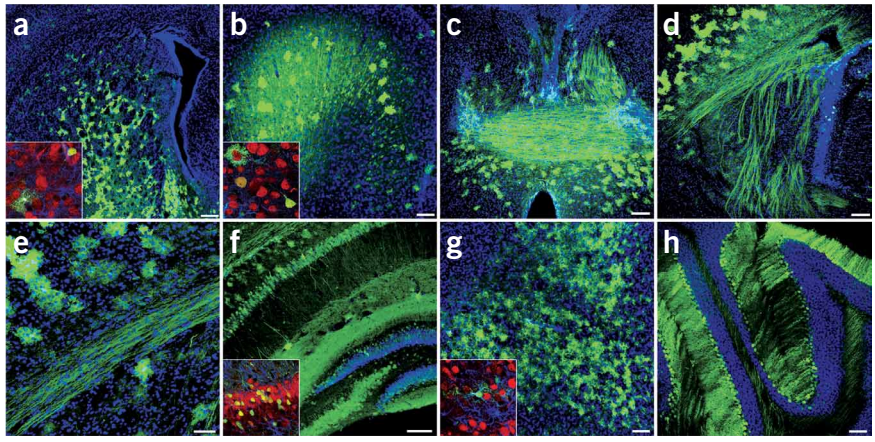

Figure 3 Widespread GFP expression 21 d after intravenous injection of 4×10^{11} particles of scAAV9-CB-GFP to postnatal-day-1 mice. (**a**–**h**) GFP localized in neurons and astrocytes throughout multiple structures of the brain ($n = 6$) as depicted in striatum (**a**), cingulate gyrus (**b**), fornix and anterior commissure (**c**), internal capsule (**d**), corpus callosum (**e**), hippocampus and dentate gyrus (**f**), midbrain (**g**) and cerebellum (**h**). All large panels show GFP (green) and DAPI (blue) merged images. Insets of selected regions show high magnification merged images of GFP (green), NeuN (red) and GFAP (blue) labeling. Schematic representations depicting the approximate locations of each image throughout the brain are shown in (**Supplementary Fig. 7** online). Higher magnification images of select structures are shown in **Figure 4**. Scale bars, 200 μm (**a**); 50 μm (**e**); 100 μm (**b**–**d**, **f**–**h**).

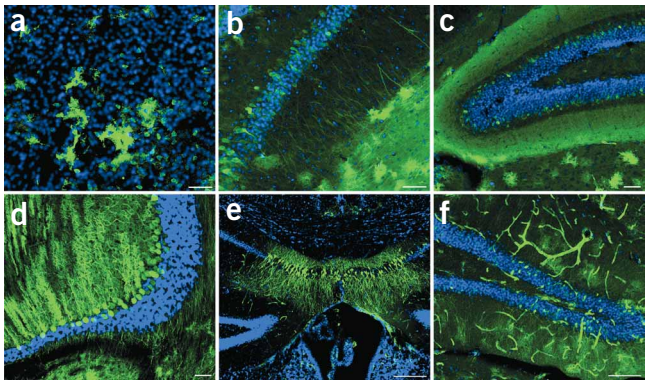

Figure 4 High magnification of merged GFP (green) and DAPI (blue) images of brain regions after intravenous injection of scAAV9-CB-GFP. (**a**–**d**) In neonates ($n = 8$), astrocytes and neurons were easily detected in the striatum (**a**), hippocampus (**b**) and dentate gyrus (**c**) after postnatal-day-1 intravenous injection of 4×10^{11} particles of scAAV9-CB-GFP. Extensive GFP expression within cerebellar Purkinje cells (**d**) was also observed. (**e**,**f**) In adults ($n = 6$), pyramidal cells of the hippocampus (**e**) and granular cells of the dentate gyrus (**f**) were the only neuronal transduction within the brain after tail vein injection. In addition to astrocyte and neuronal transduction, widespread vascular transduction (**f**) was also seen throughout all adult brain sections examined. Scale bars, 200 μm (**e**); 100 μm (**f**), 50 μm (**a**–**d**).

Astrocyte targeting in the adult spinal cord after vascular delivery

We next studied systemic delivery in adult mice by injection through the tail vein with doses ranging from 4×10^{11} to 4×10^{12} particles of scAAV9-CB-GFP (**Figs. 4e–f** and **5**). GFP expression was observed in heart and skeletal muscle, as expected (data not shown). We found a strikingly different transduction pattern in adults compared with neonates. There was an absence of GFP-positive DRG fibers and a marked decrease in LMN transduction in all cervical and lumbar spinal cord sections examined. Notably, GFP-positive astrocytes were easily observed throughout the entire dorsal-ventral extent of the gray matter in all regions of the spinal cord (**Fig. 5a–h**), with the greatest GFP-expression levels found in the higher-dosed mice. Co-labeling of GFP-positive cells with the astroglial markers excitatory amino acid transporter 2 (EAAT2) and glial fibrillary acidic protein (GFAP) demonstrated that ~90% of the GFP-positive cells were astrocytes. Counts of total astrocytes in the lumbar region of the spinal cord made in a z-series (three-dimensional) set of confocal microscopic images showed that >64% of astrocytes were positive for GFP (**Fig. 5i–l** and **Table 1**). To date, predominant glial transduction has not been reported for any AAV serotype after intravenous delivery, indicating that AAV9 has a unique transduction property in the adult CNS when delivered intravenously. We did note an occasional LMN transduced in the spinal cord, although these events were scarce in adult mice. Viral transcription was again confirmed in adult tissues with *in situ* hybridization (**Fig. 2**). Furthermore, whereas intravenous injection in neonatal mice resulted in indiscriminate astrocyte and neuronal transduction throughout the brain, tail-vein injections in adults produced isolated and localized neuronal expression only in the hippocampus and dentate gyrus (**Figs. 4e–f** and **5m,n**), in low- and high-dosed mice. Low-dosed mice had isolated patches of transduced astrocytes scattered throughout the entire brain (data not shown). Notably, high-dosed mice had extensive astrocyte and vascular transduction throughout the brain (**Figs. 4e–f** and **5m–p**) that persisted for at least 7 weeks post-injection ($n = 5$), suggesting a dose response to transduction of AAV9, without regional specificity.

Astrocyte transduction in adults is dependent on injection route

Our results show that the pattern of transduction shifted from primarily neuronal targeting in neonates to astrocytic targeting in adults. To date, we have observed the highest targeting efficiency in astrocytes. However, a recent paper reported efficient astrocyte transduction by AAV8 but not AAV9 after direct brain injection, and astrocyte transduction was suggested to be related to viral purification[20]. To investigate whether astrocyte transduction in our study was related to vector purity or delivery route, we evaluated multiple AAV9 preparations for vector purity by silver stain and injected 8×10^{10}

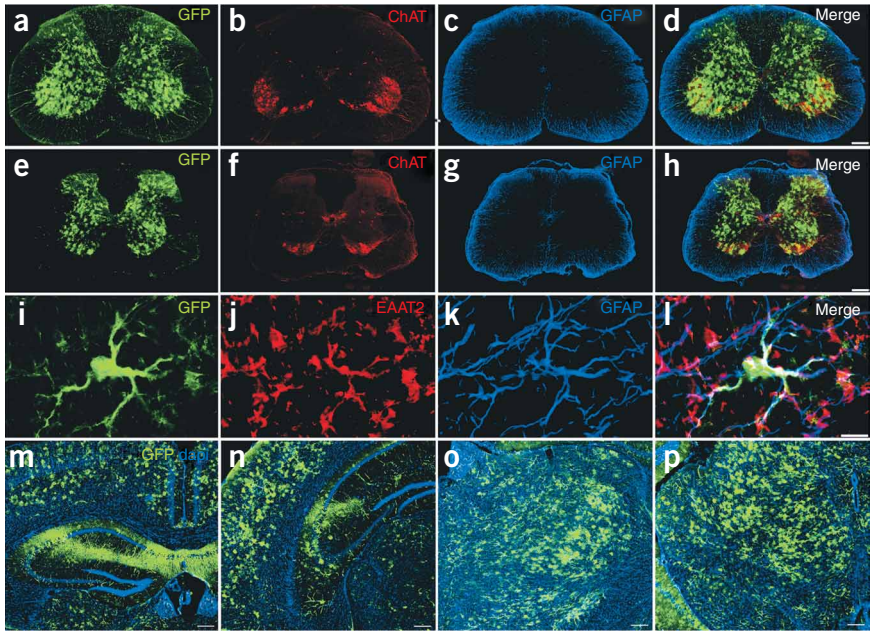

Figure 5 Intravenous injection of AAV9 leads to widespread predominant astrocyte transduction in the spinal cord and brain of adult mice. (**a**–**p**) GFP expression in the cervical (**a**–**d**) and lumbar (**e**–**h**) spinal cord as well as the brain (**m**–**p**) of adult mice 7 weeks after tail vein injection of 4×10^{12} particles of scAAV9-CB-GFP ($n = 6$). In contrast to postnatal-day-1 intravenous injections, adult tail vein injection resulted in transduction of almost exclusively astrocytes. GFP (**a**,**e**), ChAT (**b**,**f**) and GFAP (**c**,**g**) demonstrate the abundance of GFP expression throughout the spinal gray matter, with lack of co-localization with LMNs and white matter astrocytes (**d**,**h**). Co-localization of GFP (**i**), excitatory amino acid transporter 2 (EAAT2) (**j**), and GFAP (**k**) confirm that transduced cells are astrocytes (**l**). Tail vein injection also resulted in primarily astrocyte transduction throughout the brain as seen in the cortex (**m**–**n**), thalamus (**o**) and midbrain (**p**). All brain panels show GFP (green) and DAPI (blue) merged images. Neuronal GFP expression in the brain was restricted to the hippocampus and dentate gyrus (**m**–**n** and **Fig. 4e–f**). Schematic representations depicting the approximate locations of each image throughout the brain are available in **Supplementary Figure 8** online. Scale bars, 10 μm (**l**); 200 μm (**d**,**h**,**p**).

particles of the same scAAV9-CB-GFP vector preparations from the intravenous experiments into the striatum and dentate gyrus of adult mice. Silver staining showed that vector preparations were relatively pure and of research-grade quality (**Supplementary Fig. 5** online). Two weeks after intracranial injection, we observed significant neuronal transduction within the injected regions using these vector preparations. However, we found no evidence for co-localization between GFP and GFAP labeling throughout the injected brains ($n = 3$) (**Supplementary Fig. 6** online), as previously reported[21], suggesting that the astrocyte transduction in our study may be dependent on injection route and serotype and not due to vector purity.

DISCUSSION

Our findings demonstrate a unique capacity of AAV9 vectors to cross the BBB. In the neonate, intravenous delivery of AAV9-GFP resulted in widespread neuronal targeting, with an apparent tropism toward LMNs residing within the spinal cord. Substantial transduction of neurons was observed in numerous regions of the brain. GABAergic interneurons were not highly transduced by AAV9 using a vascular delivery approach, yet pyramidal and Purkinje neurons were. These transduced cells have long projection axons, unlike interneurons. Our results suggest that the specific neuroanatomy, such as neuronal morphology or vascular density, may determine which neurons are transduced by AAV9 in this injection protocol. Further study should elucidate the mechanisms by which AAV9 vectors transduce specific neuronal populations.

The scarcity of LMN and DRG transduction observed in the adult mice suggests that there is a developmental period in which access by circulating virus to these cell populations becomes restricted. Assuming a dependence on retrograde transport for DRG and LMN transduction after intravenous injection, Schwann cell or synapse maturation may be an important determinant of successful AAV9 LMN and DRG transduction. Previously, we reported retrograde transport by AAV vectors[22,23], and recently, some serotypes have demonstrated an increased capability for retrograde transport[24]. However, we did not detect obvious retrograde transport from AAV9 vectors after intramuscular injection in adult mice.

The predominant astrocyte transduction in adults suggests that AAV9 escapes brain vasculature in a similar manner as it escapes skeletal and cardiac muscle vasculature. The ability of AAV9 to penetrate or bypass endothelium is of interest. Normally, tight junctions severely restrict penetration of the BBB by molecules and viruses. AAV9 may be using transport proteins, receptor-mediated transcytosis, adsorptive transcytosis or other mechanisms to cross the BBB. Our data suggest that, after passing through the endothelial cell layer, AAV9 infects the astrocytic perivascular endfeet that surround capillary endothelial cells[25]. Our results show that astrocytes are targeted only when the virus is exposed to the astrocytic perivascular endfeet. Given that astrocytes retain some features of apical-basal polarity from development, certain receptors or channels may be accessible by this vascular entry route but not by direct intraparenchymal injections[26]. The precise mechanism of bypassing endothelial cells leading to astrocytic transduction will require further study.

In summary, our results demonstrate efficient targeting of cells within the CNS by AAV9 after intravenous delivery, particularly neurons and LMNs in the neonate and astrocytes in the adult. A simple intravenous injection of AAV9 as described here may be clinically relevant for SMA and ALS. In the context of SMA, increased expression of survival motor neuron gene (*SMN*) in LMNs may have therapeutic benefit[3,27]. Our results suggest that with a single injection, we may be able to effectively restore *SMN* expression levels in LMNs. Additionally, given the robust neuronal populations transduced throughout the CNS in neonatal mice, this approach may also allow for rapid, relatively inexpensive gene overexpression or gene knockdown[28]. Constructing AAV9-based vectors with neuronal or astrocyte-specific promoters may allow further specificity, given that AAV9 targets multiple nonneuronal tissues after intravenous delivery[11,13]. Our results also demonstrated efficient targeting of astrocytes in adult mice, and this finding may be relevant for treating ALS, where the non-cell autonomous nature of disease progression has recently been discovered, and astrocytes have been specifically linked to disease progression[29]. The ability to target astrocytes to produce trophic factors or to circumvent aberrant glial activity may be beneficial for treating ALS[30]. It is noteworthy that AAV9 vascular delivery in the adult does not achieve widespread direct neuronal targeting, precluding the use of this approach for diseases such as Huntington's, in which multiple structures and brain regions are likely to require neuronal targeting to suppress mutant Huntingtin protein[31,32]. However, viral evolution techniques may enable the generation of AAV9 variants that target adult neurons by vascular delivery[33–35]. In summary, our results highlight a relatively noninvasive method to efficiently deliver genes to the CNS that should be useful in basic and clinical neurology studies.

METHODS

All animal procedures were approved by Nationwide Children's Hospital Institutional Animal Care and Use Committee.

Virus. AAV9 was produced by transient transfection procedures using a double-stranded AAV2-ITR–based CB-GFP vector, with a plasmid encoding Rep2Cap9 sequence as previously described[16] along with an adenoviral helper plasmid pHelper (Stratagene) in 293 cells. Our serotype 9 sequence was verified by sequencing and identical to that previously described[16]. Virus was produced in three separate batches for the experiments by a contract manufacturing company (Virapur) and purified by two cesium chloride density gradient purification steps, dialyzed against PBS and formulated with 0.001% Pluronic-F68 to prevent virus aggregation and stored at 4 °C. All vector preparations were titered by quantitative PCR using Taq-Man technology. Purity of vectors was assessed by 4–12% SDS-acrylamide gel electrophoresis and silver staining (Invitrogen).

Animals. Mice used were C57Bl/6 littermates. The mother (singly housed) of each litter to be injected was removed from the cage. The postnatal-day-1 pups were rested on a bed of ice for anesthetization. For neonate injections, a light microscope was used to visualize the temporal vein (located just anterior to the ear). Vector solution was drawn into a 3/10 cc 30 gauge insulin syringe. The needle was inserted into the vein and the plunger was manually depressed. Virus injections were in a total volume of 100 µl of PBS supplemented with 0.001% pluronic-F68. A total of 4×10^{11} DNase-resistant particles of scAAV9-CB-GFP (Virapur) were injected. A correct injection was verified by noting blanching of the vein. After the injection, pups were returned to their cage. When the entire litter was injected, the pups were rubbed with bedding to prevent rejection by the mother. The mother was then reintroduced to the cage. Neonatal mice were euthanized 10 or 21 d post-injection, spinal cords and brains were extracted, rinsed in PBS, then immersion fixed in a 4% paraformaldehyde solution.

Adult tail vein injections were performed on ~70-d-old C57Bl/6 mice. Mice were placed in restraint that positioned the mouse tail in a lighted, heated groove. The tail was swabbed with alcohol then injected intravenously with a 100 µl viral solution containing a mixture of PBS and 4×10^{11}, 8×10^{11} or 4×10^{12} DNase-resistant particles of scAAV9-CB-GFP. After the injection, mice were returned to their cages. Two to seven weeks post-injection, mice were anesthetized then transcardially perfused first with 0.9% saline, then 4% paraformaldehyde. Brains and spinal cords were harvested and immersion fixed in 4% paraformaldehyde for an additional 24–48 h.

Adult intramuscular injections were performed on ~75-d-old C57Bl/6 mice as previously described[36]. Mice were anesthetized with isoflurane, and a small incision was made over the right gastrocnemius muscle. A 50 µl viral solution containing 5×10^{10} particles of scAAV9 CB GFP was injected over three sites in the gastrocnemius with a 3/10 cc 30 gauge insulin syringe. The incision was closed and the mice were allowed to recover.

Histological processing. Neonatal and adult brains were transferred from paraformaldehyde to a 30% sucrose solution for cryoprotection. The brains were mounted onto a sliding microtome with Tissue-Tek OCT compound (Sakura Finetek) and frozen with dry ice. Forty micrometer–thick sections were divided into five series for histological analysis. Tissues for immediate processing were placed in 0.01 M PBS in vials. Those for storage were placed in antifreeze solution and transferred to –20 °C. Spinal cords were cut into blocks of tissue 5–6 mm in length, and then cut into 40 µ thick transverse sections on a vibratome (Leica). Serial sections were kept in a 96-well plate that contained 4% paraformaldehyde and were stored at 4 °C.

Muscles were dissected, snap-frozen in liquid nitrogen-cooled isopentane, cryostat sectioned and mounted onto slides for observation of GFP fluorescence.

Immunohistochemistry. Brains and spinal cords were stained as floating sections. Brains were stained in a 12-well dish, and spinal cords sections were stained in a 96-well plate to maintain their rostral-caudal sequence. Tissues were washed three times for 5 min each in PBS, then blocked in a solution containing 10% donkey serum and 1% Triton X-100 for 2 h at 25 °C. After blocking, antibodies were diluted in the blocking solution at 1:500. The primary antibodies used were as follows: goat anti-ChAT and mouse anti-NeuN (Millipore), rabbit anti-GFP (Invitrogen), guinea pig anti-GFAP (Advanced Immunochemical) and goat anti-GAD67 (Millipore). Biotinylated tomato lectin (Vector Labs) and isolectin B_4 (Sigma-Aldrich) were treated as primary antibodies during tissue incubation. Tissues were incubated in primary antibody at 4 °C for 48–72 h then washed three times with PBS. After washing, tissues were incubated for 2 h at 25 °C in the appropriate secondary antibodies or streptavidin-conjugated fluorophores (1:125 Jackson Immunoresearch) with DAPI. Tissues were then washed three times with PBS, mounted onto slides then coverslipped. All images were captured on a Zeiss laser scanning confocal microscope.

***In situ* hybridization.** Using a plasmid which contained T3- and T7-promoter sequences with a cloned GFP gene, we generated by PCR antisense and sense DIG-UTP–labeled GFP riboprobes. Probe yield and incorporation of DIG-UTP was confirmed by electrophoresis and dot blot. Sections of spinal cord 10 µm-thick were mounted on SuperFrost slides and prepared by fixation with 4% paraformaldehyde, washed in 0.5× SSC, permeabilized by incubation in proteinase K (2.5 µg/ml), washed in 0.5× SSC and dehydrated in series of alcohol washes. Prehybridization was performed at 42 °C using RiboHybe buffer (Ventana) for 1 h followed by hybridization overnight at 55 °C with the respective riboprobes on AAV9-injected and PBS-control-injected neonatal and adult cord sections. Stringency washes were performed and immunological detection using anti-Digoxigenin AP antibody (1:500, Roche) and development with NBT/BCIP (Pierce) and Nuclear Fast Red (Vector).

Stereology and LMN and astrocyte quantification. Stereology for total number of neurons in a given area and total number of GFP-positive cells was carried out on a Nikon E800 fluorescent microscope with computer-assisted microscopy and image analysis using StereoInvestigator software (MicroBrightField) with the optical dissector principle to avoid oversampling errors and the Cavalieri estimation for volumetric measurements. Coronal 40 µm sections, 240 µm apart covering the regions of interest in its rostro-caudal extension were evaluated. The entire dentate gyrus, caudal retrosplenial/cingulate cortex, containing the most caudal extent of the dentate gyrus, extending medially to the subiculum and laterally to the occipital cortex, and the Purkinje cell layer was sampled using ~15–25 optical dissectors in each case. Fluorescent microscopy using a 60× objective for NeuN and GFP were used and cells within the optical dissector were counted on a computer screen. Neuronal density and positive GFP density were calculated by multiplying the total volume to estimate the percent of neuronal transduction in each given area as previously described[37]. The volume of the granule cell layer was $1.76 \times 108 \pm 0.11 \times 108$ µm^3 and $1.95 \times 108 \pm 0.17$ µm^3. The sample volume was 9,000 µm^3. The Purkinje cell layer volume was 3,870 µm^3 ± 195 µm^3 for 10 d and 4,135 µm^3 ± 98 µm^3. The coefficient of error for the cell counts ranged from 0.05 to 0.10. Statistical analysis showed no differences between 10 and 21 d post-injection for any structure analyzed.

For LMN quantification, serial 40 µm thick lumbar spinal cord sections, each separated by 480 µm, were labeled as described for GFP and ChAT expression. Stained sections were serially mounted on slides from rostral to caudal, then coverslipped. Sections were evaluated using confocal microscopy (Zeiss) with a 40× objective and simultaneous FITC and Cy3 filters. FITC was visualized through a 505–530 nm band pass filter to avoid contaminating the Cy3 channel. The total number of ChAT-positive cells found in the ventral horns with defined soma was tallied by careful examination through the entire z-extent of the section. GFP-labeled cells were quantified in the same manner, while checking for co-localization with ChAT. The total number of cells counted per animal ranged from ~150 to 366 cells per animal. For astrocyte quantification, as with LMNs, serial sections were stained for GFP, GFAP and EAAT2, then mounted. Using confocal microscopy with a 63× objective and simultaneous FITC and Cy5 filters, random fields in the ventral horns of lumbar spinal cord sections from tail vein–injected mice were selected. The total numbers of GFP- and GFAP-positive cells were counted from a minimum of at least 24 fields per animal while focusing through the entire z extent of the section.

Statistical Analysis. Statistical analyses were performed using Graph Pad Prizm software. Means were represented with s.e.m. Student's *t*-tests were performed to compare 10 versus 21 d post-injection using a 95% confidence level.

Note: Supplementary information is available on the Nature Biotechnology website.

ACKNOWLEDGMENTS

This work was supported by National Institutes of Health (NIH)/National Eye Institute (NEI) R21EY018491, NIH/National Institute of Neurological Disorders and Stroke (NINDS) R21NS064328, Project A.L.S. and The Muscular Dystrophy Association. We kindly thank Jeff Rothstein (Johns Hopkins University) for the EAAT2 antibody, Terri Shaffer (Nationwide Children's Hospital) for expertise in mouse tail vein injections, Michele Basso (Ohio State University) and Megan Detloff (Ohio State University) for stereology usage and advice and Phillip Popovich (Ohio State University) and Kristina Kigerl (Ohio State University) for expertise in microglial detection.

AUTHOR CONTRIBUTIONS

K.D.F. and B.K.K. designed and executed experiments and wrote the manuscript. E.N. contributed to animal and histological experiments. C.L.M. performed adult tail vein injections. A.H. and C.M.C. performed *in situ* hybridization.

COMPETING INTERESTS STATEMENT

The authors declare competing financial interests: details accompany the full-text HTML version of the paper at http://www.nature.com/naturebiotechnology/

Published online at http://www.nature.com/naturebiotechnology/
Reprints and permissions information is available online at http://npg.nature.com/reprintsandpermissions/

1. Pardridge, W.M. Drug and gene targeting to the brain with molecular Trojan horses. *Nat. Rev. Drug Discov.* **1**, 131–139 (2002).
2. Kaspar, B.K., Llado, J., Sherkat, N., Rothstein, J.D. & Gage, F.H. Retrograde viral delivery of IGF-1 prolongs survival in a mouse ALS model. *Science* **301**, 839–842 (2003).
3. Azzouz, M. *et al.* Lentivector-mediated SMN replacement in a mouse model of spinal muscular atrophy. *J. Clin. Invest.* **114**, 1726–1731 (2004).
4. Azzouz, M. *et al.* VEGF delivery with retrogradely transported lentivector prolongs survival in a mouse ALS model. *Nature* **429**, 413–417 (2004).
5. Ralph, G.S. *et al.* Silencing mutant SOD1 using RNAi protects against neurodegeneration and extends survival in an ALS model. *Nat. Med.* **11**, 429–433 (2005).
6. Kaplitt, M.G. *et al.* Safety and tolerability of gene therapy with an adeno-associated virus (AAV) borne GAD gene for Parkinson's disease: an open label, phase I trial. *Lancet* **369**, 2097–2105 (2007).
7. Marks, W.J. Jr. *et al.* Safety and tolerability of intraputaminal delivery of CERE-120 (adeno-associated virus serotype 2-neurturin) to patients with idiopathic Parkinson's disease: an open-label, phase I trial. *Lancet Neurol.* **7**, 400–408 (2008).
8. Worgall, S. *et al.* Treatment of late infantile neuronal ceroid lipofuscinosis by CNS administration of a serotype 2 adeno-associated virus expressing CLN2 cDNA. *Hum. Gene Ther.* **19**, 463–474 (2008).

9. Blankinship, M.J. *et al.* Efficient transduction of skeletal muscle using vectors based on adeno-associated virus serotype 6. *Mol. Ther.* **10**, 671–678 (2004).
10. Wang, Z. *et al.* Adeno-associated virus serotype 8 efficiently delivers genes to muscle and heart. *Nat. Biotechnol.* **23**, 321–328 (2005).
11. Inagaki, K. *et al.* Robust systemic transduction with AAV9 vectors in mice: efficient global cardiac gene transfer superior to that of AAV8. *Mol. Ther.* **14**, 45–53 (2006).
12. Nakai, H. *et al.* Unrestricted hepatocyte transduction with adeno-associated virus serotype 8 vectors in mice. *J. Virol.* **79**, 214–224 (2005).
13. Pacak, C.A. *et al.* Recombinant adeno-associated virus serotype 9 leads to preferential cardiac transduction in vivo. *Circ. Res.* **99**, e3–e9 (2006).
14. Towne, C., Raoul, C., Schneider, B.L. & Aebischer, P. Systemic AAV6 delivery mediating RNA interference against SOD1: neuromuscular transduction does not alter disease progression in fALS mice. *Mol. Ther.* **16**, 1018–1025 (2008).
15. Foust, K.D., Poirier, A., Pacak, C.A., Mandel, R.J. & Flotte, T.R. Neonatal intraperitoneal or intravenous injections of recombinant adeno-associated virus type 8 transduce dorsal root ganglia and lower motor neurons. *Hum. Gene Ther.* **19**, 61–70 (2008).
16. Gao, G. *et al.* Clades of Adeno-associated viruses are widely disseminated in human tissues. *J. Virol.* **78**, 6381–6388 (2004).
17. Cearley, C.N. & Wolfe, J.H. Transduction characteristics of adeno-associated virus vectors expressing cap serotypes 7, 8, 9, and Rh10 in the mouse brain. *Mol. Ther.* **13**, 528–537 (2006).
18. Akache, B. *et al.* The 37/67-kilodalton laminin receptor is a receptor for adeno-associated virus serotypes 8, 2, 3, and 9. *J. Virol.* **80**, 9831–9836 (2006).
19. McCarty, D.M. *et al.* Adeno-associated virus terminal repeat (TR) mutant generates self-complementary vectors to overcome the rate-limiting step to transduction in vivo. *Gene Ther.* **10**, 2112–2118 (2003).
20. Klein, R.L., Dayton, R.D., Tatom, J.B., Henderson, K.M. & Henning, P.P. AAV8, 9, Rh10, Rh43 vector gene transfer in the rat brain: effects of serotype, promoter and purification method. *Mol. Ther.* **16**, 89–96 (2008).
21. Cearley, C.N. *et al.* Expanded repertoire of AAV vector serotypes mediate unique patterns of transduction in mouse brain. *Mol. Ther.* **16**, 1710–1718 (2008).
22. Kaspar, B.K. *et al.* Targeted retrograde gene delivery for neuronal protection. *Mol. Ther.* **5**, 50–56 (2002).
23. Miller, T.M. *et al.* Gene transfer demonstrates that muscle is not a primary target for non-cell-autonomous toxicity in familial amyotrophic lateral sclerosis. *Proc. Natl. Acad. Sci. USA* **103**, 19546–19551 (2006).
24. Hollis, E.R., II, Kadoya, K., Hirsch, M., Samulski, R.J. & Tuszynski, M.H. Efficient retrograde neuronal transduction utilizing self-complementary AAV1. *Mol. Ther.* **16**, 296–301 (2008).
25. Abbott, N.J., Ronnback, L. & Hansson, E. Astrocyte-endothelial interactions at the blood-brain barrier. *Nat. Rev. Neurosci.* **7**, 41–53 (2006).
26. Abbott, N.J. Dynamics of CNS barriers: evolution, differentiation, and modulation. *Cell. Mol. Neurobiol.* **25**, 5–23 (2005).
27. Baughan, T. *et al.* Stimulating full-length SMN2 expression by delivering bifunctional RNAs via a viral vector. *Mol. Ther.* **14**, 54–62 (2006).
28. Siegel, R.M. & Callaway, E.M. Francis Crick's legacy for neuroscience: between the alpha and the Omega. *PLoS Biol.* **2**, e419 (2004).
29. Yamanaka, K. *et al.* Astrocytes as determinants of disease progression in inherited amyotrophic lateral sclerosis. *Nat. Neurosci.* **11**, 251–253 (2008).
30. Dodge, J.C. *et al.* Delivery of AAV-IGF-1 to the CNS extends survival in ALS mice through modification of aberrant glial cell activity. *Mol. Ther.* **16**, 1056–1064 (2008).
31. Harper, S.Q. *et al.* RNA interference improves motor and neuropathological abnormalities in a Huntington's disease mouse model. *Proc. Natl. Acad. Sci. USA* **102**, 5820–5825 (2005).
32. Rodriguez-Lebron, E., Denovan-Wright, E.M., Nash, K., Lewin, A.S. & Mandel, R.J. Intrastriatal rAAV-mediated delivery of anti-huntingtin shRNAs induces partial reversal of disease progression in R6/1 Huntington's disease transgenic mice. *Mol. Ther.* **12**, 618–633 (2005).
33. Maheshri, N., Koerber, J.T., Kaspar, B.K. & Schaffer, D.V. Directed evolution of adeno-associated virus yields enhanced gene delivery vectors. *Nat. Biotechnol.* **24**, 198–204 (2006).
34. Li, W. *et al.* Engineering and selection of shuffled AAV genomes: a new strategy for producing targeted biological nanoparticles. *Mol. Ther.* **16**, 1252–1260 (2008).
35. Koerber, J.T., Jang, J.H. & Schaffer, D.V. DNA shuffling of adeno-associated virus yields functionally diverse viral progeny. *Mol. Ther.* **16**, 1703–1709 (2008).
36. Haidet, A.M. *et al.* Long-term enhancement of skeletal muscle mass and strength by single gene administration of myostatin inhibitors. *Proc. Natl. Acad. Sci. USA* **105**, 4318–4322 (2008).
37. Kempermann, G., Kuhn, H.G. & Gage, F.H. Genetic influence on neurogenesis in the dentate gyrus of adult mice. *Proc. Natl. Acad. Sci. USA* **94**, 10409–10414 (1997).

Supplementary Figure 1

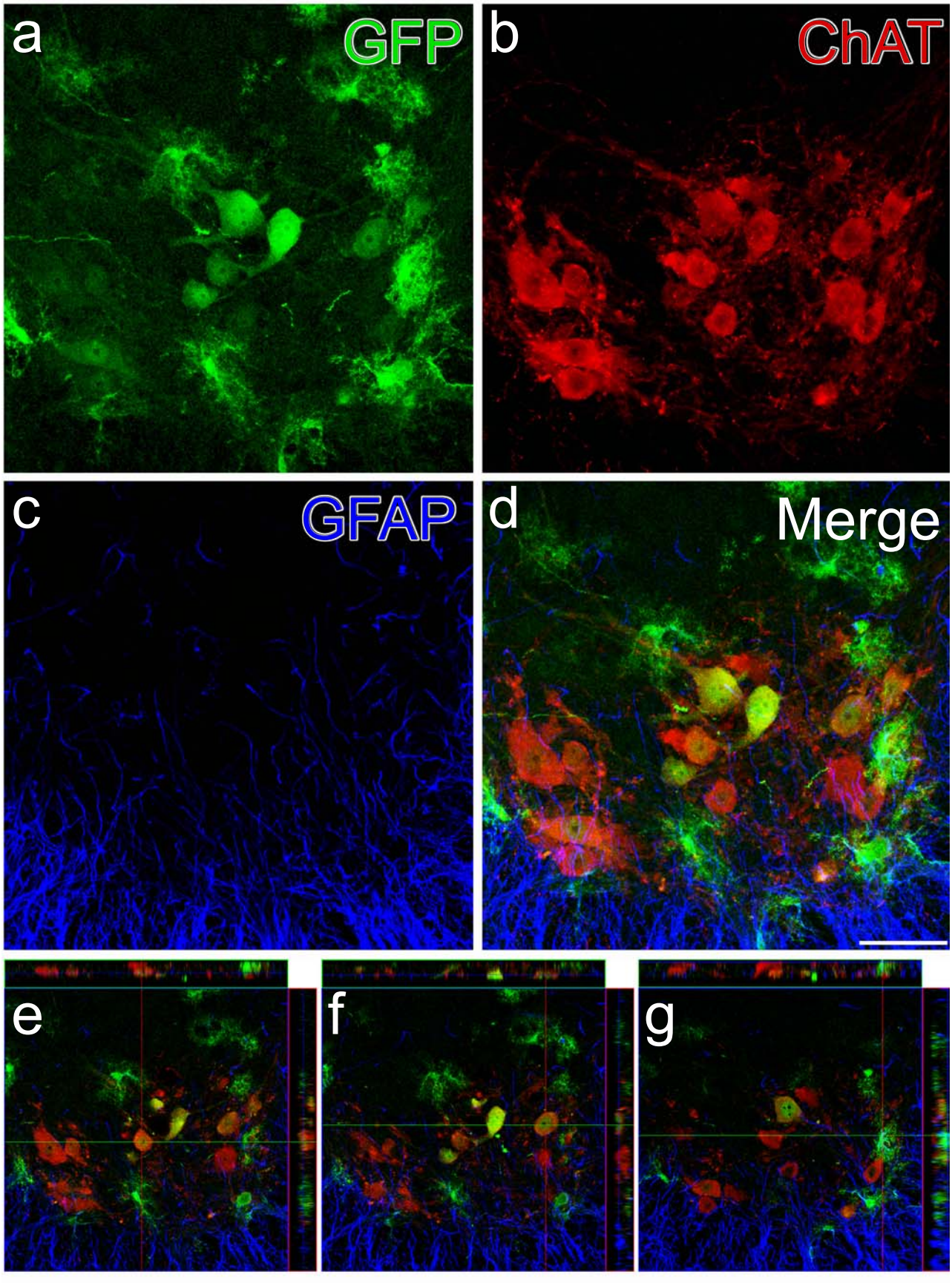

Supplementary Figure 1 Intravenous injection of AAV9 leads to widespread and long-term neonatal spinal cord transduction in lumbar motor neurons. Z-series confocal microscopy showing GFP-expression in 21-day-old mice that received $4x10^{11}$ particles of scAAV9-CB-GFP intravenous injections on postnatal day-1. Z-stack images of GFP (**a**), ChAT (**b**), GFAP (**c**) and merged (**d**) demonstrating persistent GFP-expression in motor neurons and astrocytes (**d**) for at least three-weeks following scAAV9-CB-GFP injection. Orthoganol views (**e-g**) further confirm co-localization between GFP and ChAT labeled cells (**e-f**) and a GFP and GFAP labeled cell (**g**). Scale bar, 20μm (**d**).

Supplementary Figure 2

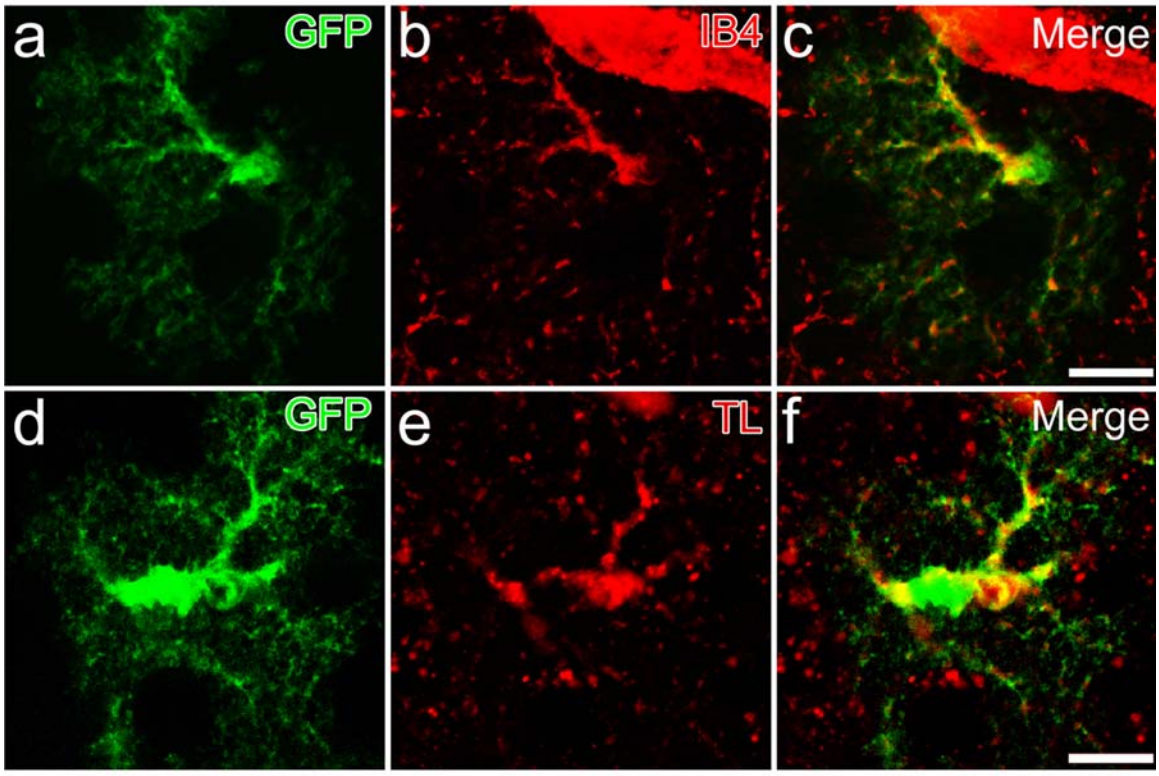

Supplementary Figure 2 Intravenous injection of scAAV9 CB GFP resulted in GFP expression within microglia 21 days after postnatal day-1 administration. Immunofluorescent detection of GFP (**a,d**) and isolectin B_4 (**b**) or tomato lectin (**e**) mediated labeling demonstrates AAV9 transduction of microglia (**c,f**) in the neonate. Scale bars, 10μm (**c** and **f**)

Nature Biotechnology: doi:10.1038/nbt.1515

Supplementary Figure 3

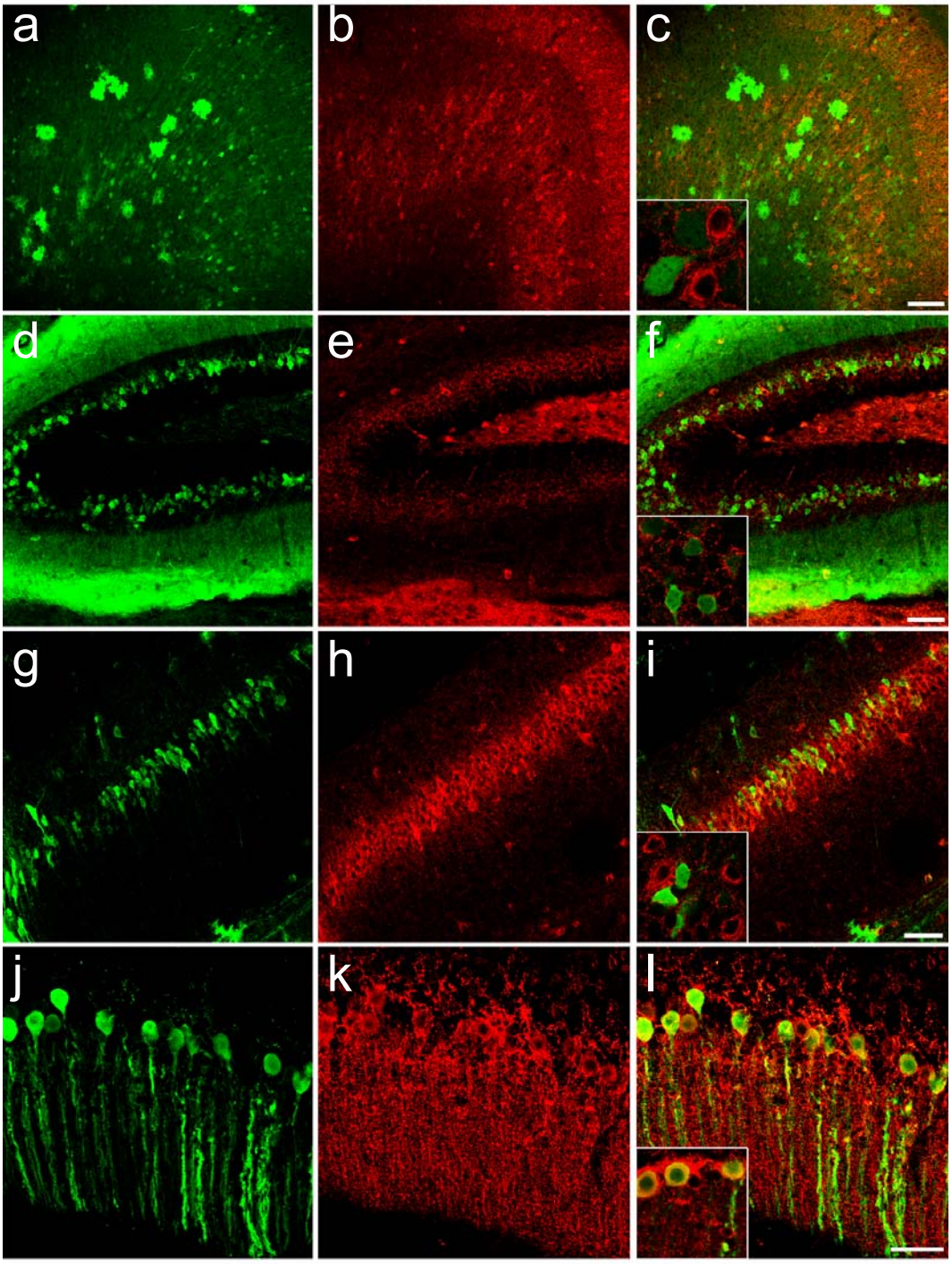

Supplementary Figure 3 Co-localization of GFP positive cells with GAD67. Immunohistochemical detection of GFP (**a**,**d**,**g**,**j**) and GAD67 (**b**,**e**,**h**,**k**) expression within select regions of mouse brain 21-days following postnatal day-1 injection of $4x10^{11}$ particles of scAAV9-CB-GFP. Merged images (**c**,**f**,**i**,**l**) and insets show limited co-localization of GFP and GAD67 signals in the cingulate gyrus (**a-c**), the dentate gyrus (**d-f**) and the hippocampus (**g-i**), but numerous GFP/GAD67 Purkinje cells within the cerebellum(**l**). Scale bars, 100μm (**c**), 50μm (**a-b**,**d-l**)

Nature Biotechnology: doi:10.1038/nbt.1515

Supplementary Figure 4

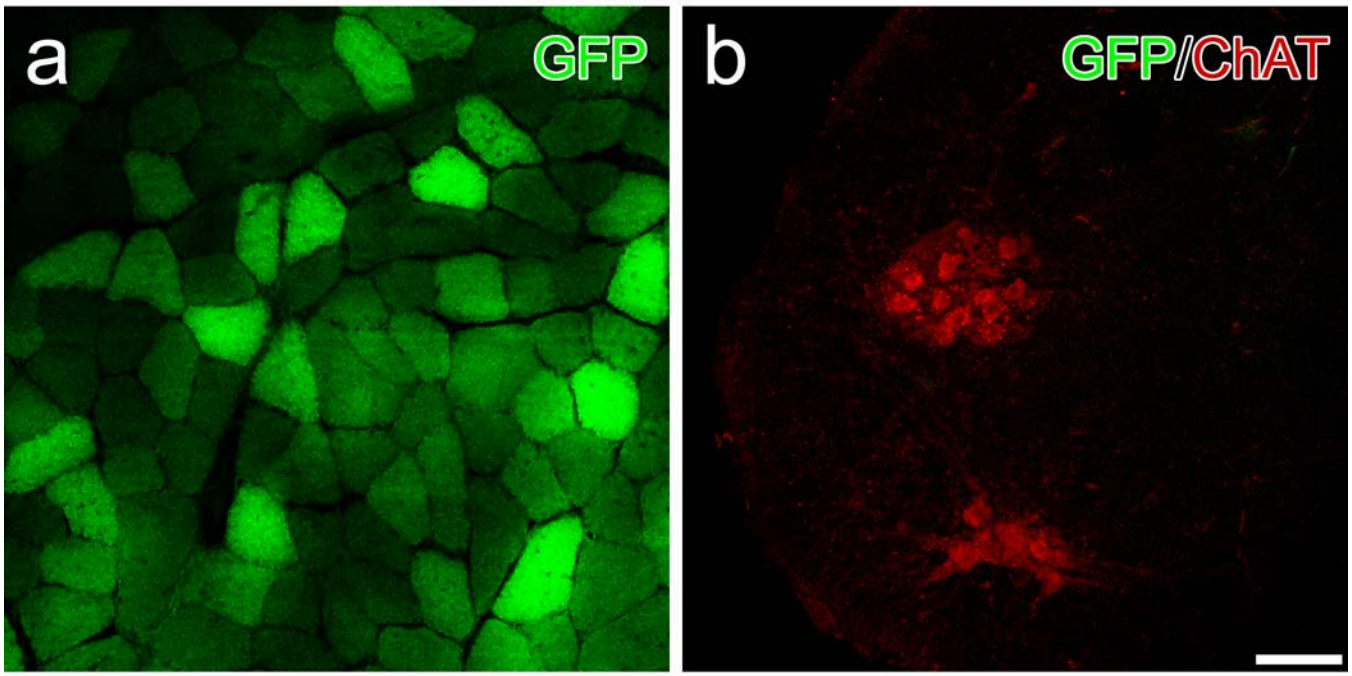

Supplementary Figure 4 Intramuscular injection of scAAV9 CB GFP resulted in robust GFP expression in the injected muscle (**a**) but a lack of expression within innervating lower motor neurons (**b**). Tissues were harvested two-weeks post intramuscular injection of $5x10^{10}$ particles of scAAV9 CB GFP. Scale bar, 100μm (**b**)

Nature Biotechnology: doi:10.1038/nbt.1515

Supplementary Figure 5

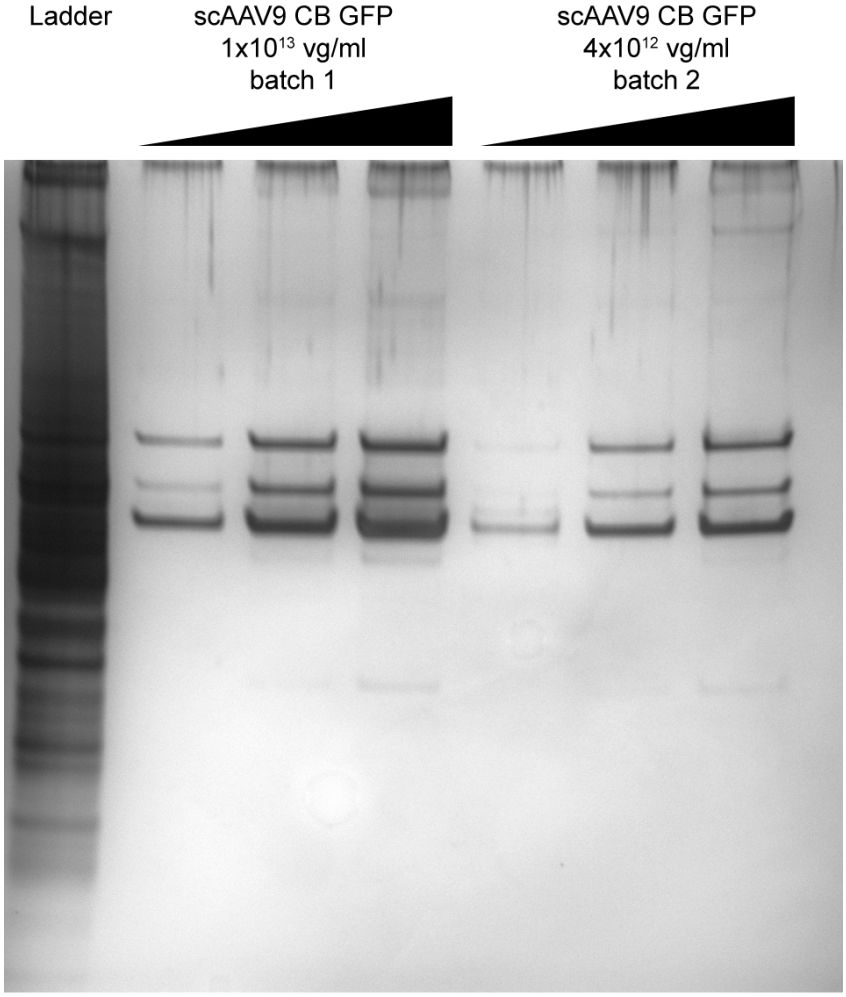

Supplementary Figure 5 Gel Electrophoresis and silver staining of various AAV9-CB-GFP vector preparations demonstrates high purity of research grade virus utilized in studies. Shown are 2 vector batches at varying concentrations demonstrating the predominant 3 viral proteins (VP); VP1, 2, 3 as the significant components of the preparation. 1µl, 5µl, and 10µl were loaded of each respective batch of virus.

Nature Biotechnology: doi:10.1038/nbt.1515

Supplementary Figure 6

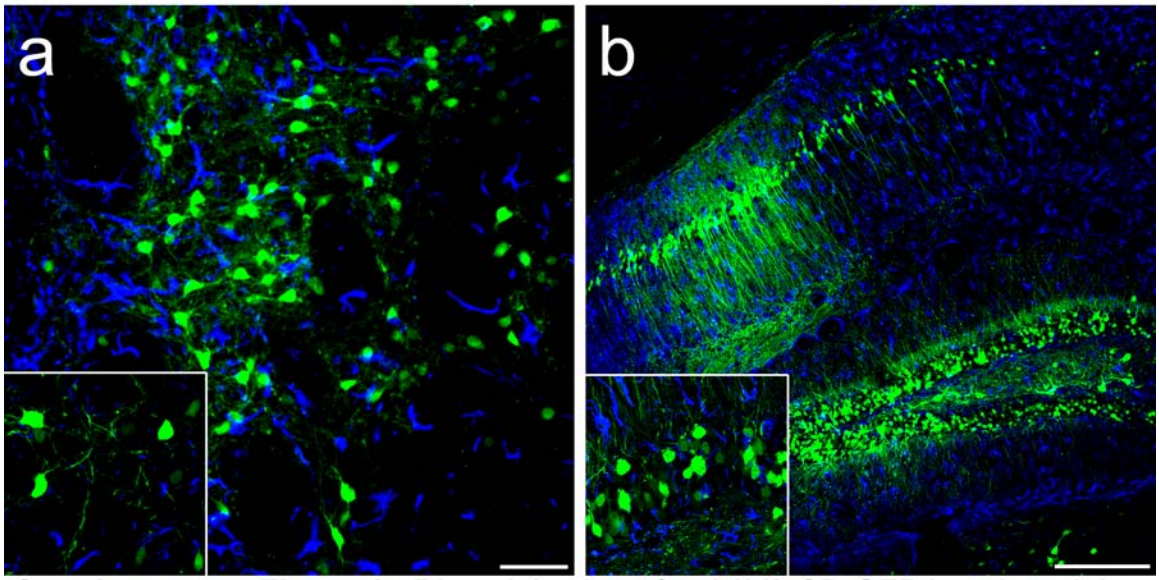

Supplementary Figure 6 Direct injection of scAAV9-CB-GFP into the adult brain demonstrates predominant neuronal transduction. Injection of virus into the striatum (**a**) and hippocampus (**b**) resulted in the familiar neuronal transduction pattern as expected (*n*=3). Co-labeling for GFP (green) and GFAP (blue) demonstrate a lack of astrocyte transduction in the injected structures with significant neuronal cell transduction. Insets of striatum (**a**) and dentate gyrus (**b**) show high magnification merged images of GFP (green) and GFAP (blue) labeling futher confirming a lack of astrocyte transduction. Scale bars, 50μm (**a**), 200μm (**b**)

Supplementary Figure 7

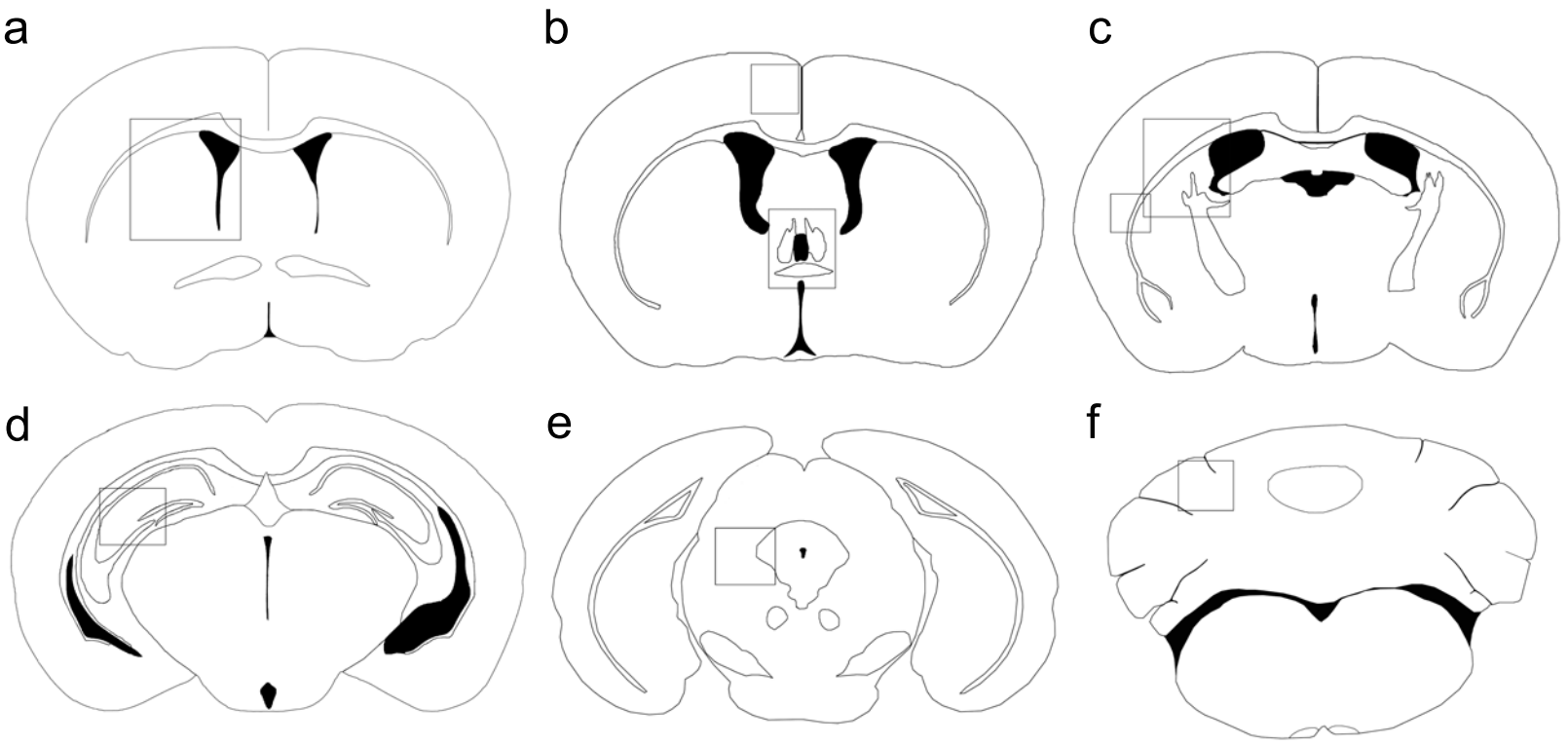

Supplementary Figure 7 Diagrams of coronal sections throughout the mouse brain corresponding to the approximate locations shown in **figure 3**(**a-h**) for postnatal day-1 injected neonatal mouse brains. The box in (**a**) corresponds to the location of (**Fig. 3a**). The smaller box in (**b**) corresponds to (**Fig. 3b**) and the larger box to (**Fig. 3c**). The larger box in (**c**) corresponds to (**Fig. 3d**) while the smaller box in (**c**) represents (**Fig. 3e**). Finally, (**d-f**) correspond to (**Fig. 3 f-h**) respectively.

Nature Biotechnology: doi:10.1038/nbt.1515

Supplementary Figure 8

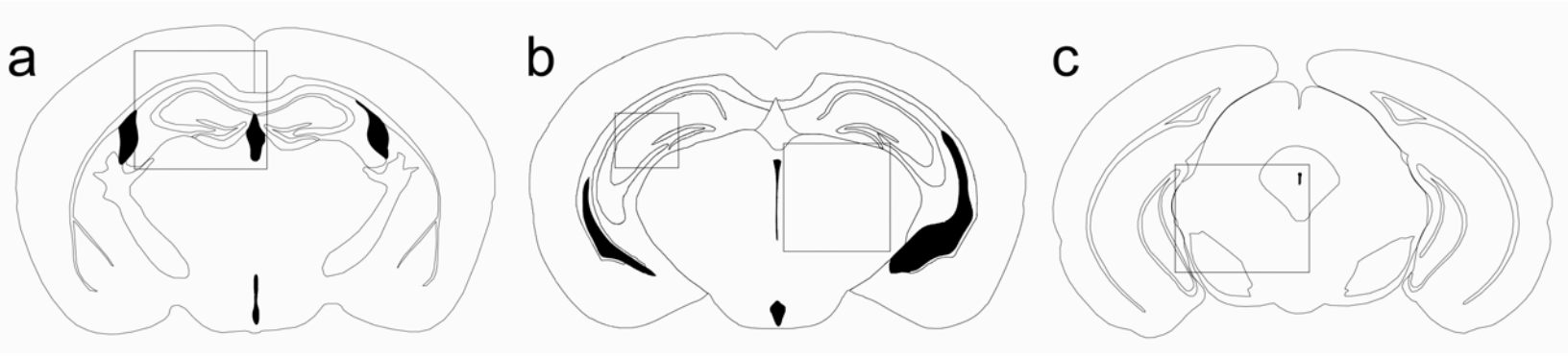

Supplementary Figure 8 Diagrams of coronal sections throughout the mouse brain corresponding to the approximate locations shown in (**Fig. 5m-p**). The box in (**a**) corresponds to the location shown in (**Fig. 5m**). The smaller box in (**b**) corresponds to (**Fig. 5n**) and the larger box to (**Fig. 5o**). Finally, the approximate location of (**Fig. 5p**) is shown in (**c**).

Nature Biotechnology: doi:10.1038/nbt.1515